ACS APPLIED MATERIALS & INTERFACES
RESEARCH ARTICLE
www.acsami.org

High Temperature Polyimide Containing Anthracene Moiety and Its Structure, Interface, and Nonvolatile Memory Behavior

Samdae Park,† Kyungtae Kim,† Dong Min Kim, Wonsang Kwon, Junman Choi, and Moonhor Ree*

Division of Advanced Materials Science, Department of Chemistry, Pohang Accelerator Laboratory,
Center for Electro-Photo Behaviors in Advanced Molecular Systems, BK School of Molecular Science, and
Polymer Research Institute, Pohang University of Science and Technology (POSTECH), Pohang 790-784, Republic of Korea

S *Supporting Information*

ABSTRACT: A high temperature polyimide bearing anthracene moieties, poly(3,3′-di(9-anthracenemethoxy)-4,4′-biphenylene hexafluoroisopropylidenediphthalimide) (6F-HAB-AM PI) was synthesized. The polymer exhibits excellent thermal stability up to around 410 °C. This polymer is amorphous but orients preferentially in the plane of nanoscale thin films. In device fabrications of its nanoscale thin films with metal top and bottom electrodes, no diffusion of the metal atoms or ions between the polymer and electrodes was found; however, the aluminum bottom electrode had somewhat undergone oxide layer (about 1.2 nm thick) formation at the surface during the post polymer layer formation process, which was confirmed to have no significant influence on the device performance. The polymer thin film exhibited excellent unipolar and bipolar switching behaviors over a very small voltage range, less than ±2 V. Further, the PI films show repeatable writing, reading, and erasing ability with long reliability and high ON/OFF current ratio (up to 10^7) in air ambient conditions as well as even at temperatures up to 200 °C.

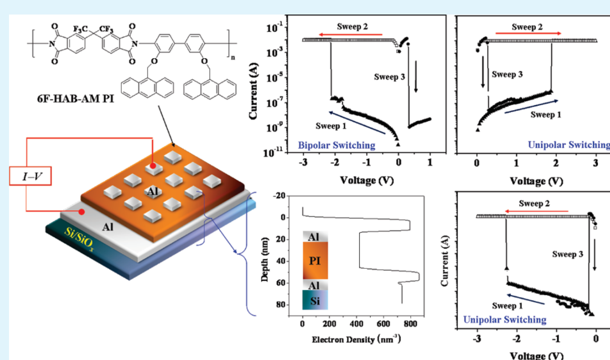

KEYWORDS: high temperature polyimide, anthracene moiety, nanoscale thin film, amorphous, in-plane orientation, nonvolatile polymer memory, bipolar switching, unipolar switching, space-charge-limited current, local filament formation

INTRODUCTION

Electrical switching phenomena in organic and polymeric materials have gained much attention for last three decades because they can easily be miniaturized in memory device applications, and furthermore, their properties can easily be tailored through chemical synthesis.[1−3] Anthracene is a good example of an organic material which reveals electrical switching behavior.[2] Anthracene films with a thickness of less than 5 μm demonstrated electrically ON and OFF bistable switching behavior, depending on electrodes in devices. However, organic materials are mostly insoluble in common solvents suitable for a coating process and, thus, require more elaborate and more expensive fabrication processes such as monolayer formation via chemical surface tethering to substrates[4] and vacuum evaporation and deposition that are commonly used in the fabrication of inorganic materials.[1,2] Moreover, deposited organic layers have relatively low boiling points and low chemical resistances, which means that they are susceptible to damage during the processing required by the fabrication of memory devices.[3]

In contrast, polymeric materials exhibit easy processability, flexibility, high mechanical strength, and good scalability. Further, they can be processed at low cost, and the multistack layer structures required for highly dense memory devices can easily be fabricated from them. Therefore, there is currently much research into the development of polymer switching materials with properties and processability that meet the requirements of the production of nonvolatile memory devices. As a result, several such polymer materials have been reported so far.[5−12] However, most of these polymers have aliphatic hydrocarbon backbones with low dimensional stability,[5,6,8,9] and they exhibit high ON and OFF switching voltages[8,9] as well as high OFF currents.[8] In particular, poly(methylmethacrylate-*co*-9-anthracenylmethylmethacrylate) (whose molar chemical composition ratio is 10:1), an aliphatic polymer containing anthracene moiety, was found to show electrical instability when its device was operated in ambient air.[5] Its electrical switching mechanism, however, was not investigated in detail. Thus, the development of nonvolatile memory devices based on dimensionally and thermally stable high performance polymers remains in the exploration stage.

In this study, we report the synthesis of a new anthracene containing polyimide (PI), poly(3,3′-di(9-anthracenemethoxy)-4,4′-biphenylene hexafluoroisopropylidenediphthalimide)

Received: November 17, 2010
Accepted: January 31, 2011
Published: February 21, 2011

© 2011 American Chemical Society

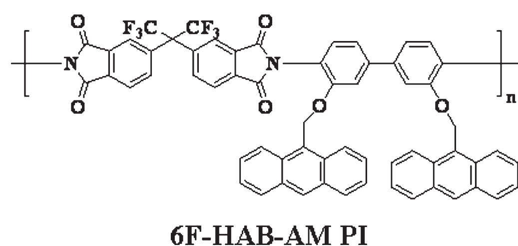

Figure 1. Chemical structure of the aromatic polyimide, 6F-HAB-AM PI.

(6F-HAB-AM PI; Figure 1) and its structure and properties including nonvolatile memory characteristics. This PI is soluble in common solvents and, therefore, easily fabricated by means of conventional solution spin-coating (or roll- or dip-coating) and subsequent drying, producing high quality nanoscale thin films that exhibit excellent thermal and dimensional stability. The polymer is amorphous but reveals relatively high in-plane orientation in nanoscale thin films. The PI devices with metal electrodes demonstrate excellent nonvolatile bipolar and unipolar switching behaviors with a high ON/OFF ratio and long retention time in ambient air conditions and even at high temperatures up to 200 °C, which can be produced in three-dimensional arrays for very high density storage. In addition, the switching mechanism of the nonvolatile memory devices is investigated. Furthermore, the interface of the polymer films in contact with metal electrodes is examined and correlated to the device performance.

EXPERIMENTAL SECTION

2,2′-Bis-(3,4-dicarboxyphenyl)hexafluoropropane dianhydride (6F) and 3,3′-dihydroxy-4,4′-diphenylene diamine (HAB) were purchased from Fluorochem Company and Chriskev Company, respectively. 6F was purified by recrystallization from acetic anhydride, and HAB was dried at 100 °C under vacuum for 1 day. All other materials were purchased from Aldrich and used as received.

A soluble PI, poly(3,3′-dihydroxy-4,4′-biphenylene hexafluoroisopropylidenediphthalimide) (6F-HAB PI) was synthesized in *N*-methyl-2-pyrrolidone (NMP) as follows: The dianhydride (6F, 5.000 g, 11.26 mmol) and diamine (HAB, 2.430 g, 11.26 mmol) were dissolved together in dry NMP with isoquinoline (2.53 mL) as a catalyst. The reaction mixture was gently heated to 70 °C under stirring for 2 h, followed by refluxing for 5 h. The reaction solution was then poured into a mixture of methanol and water under vigorous stirring. The precipitate was filtered, then washed with methanol, and dried under vacuum, giving the target PI product with a yield of 98%. The obtained PI was identified by proton nuclear magnetic resonance (^{1}H NMR) spectroscopy. ^{1}H NMR (δ in ppm, dimethyl-d_6 sulfoxide (DMSO-d_6)): 10.10 (s, 1H, Ar-OH), 8.24 (d, 1H, Ar-H), 8.03 (d, 1H, Ar-H), 7.82 (d, 1H, Ar-H), 7.43 (d, 1H, Ar-H), 7.23 (d, 2H, Ar-H).

The obtained 6F-HAB PI was further reacted to give the desired product, 6F-HAB-AM PI, as follows. 6F-HAB PI (0.624 g, 1.00 mmol), anthracenemethanol (AM) (0.624 g, 3.00 mmol), and triphenylphosphine (0.786 g, 3.00 mmol) were dissolved in dry tetrahydrofuran under nitrogen atmosphere. Then, diisopropyl azodicarboxylate (DIAD, 0.606 g, 3.00 mmol) was added dropwise. The mixture was stirred at room temperature for 24 h. The solution was poured into methanol under vigorous stirring, giving 6F-HAB-AM PI in powder. The precipitate was filtered, washed with methanol, and dried under vacuum to give a yield of 85%. ^{1}H NMR (δ in ppm, DMSO-d_6): 8.61−7.40 (m, 30H, Ar-OH), 6.30 (br, 4H, CH_2O).

Molecular weights were measured using a gel permeation chromatography (GPC) system (model PL-GPC 210, Polymer Laboratories, England) calibrated with polystyrene standards. In the GPC measurements, a flow rate of 1.0 mL/min was employed and tetrahydrofuran (THF) was used as the eluent. Thermogravimetric analysis (TGA) and differential scanning calorimetry (DSC) measurements were carried out under a nitrogen atmosphere using a thermogravimeter (model TG/DTA 6200, Seiko Instruments, Japan) and a calorimeter (model DSC 6200, Seiko Instruments, Japan). A rate of 10.0 °C/min was employed for heating and cooling runs.

Optical properties were measured using an ultraviolet−visible (UV−vis) spectrometer (Scinco model S-3100). Cyclic voltammetry (CV) was carried out in 0.1 M tetrabutylammonium tetrafluoroborate in acetonitrile using an electrochemical workstation (IM6ex impedance analyzer) with a platinum gauze counter electrode and an Ag/AgCl (saturated KCl) reference electrode, and the polymer was coated on the gold (Au) electrode deposited on silicon wafer. A scan rate of 100 mV/s was used.

Thin films of the 6F-HAB-AM PI polymer and their devices were prepared as follows. One wt % solution of the polymer in cyclopentanone was filtered through polytetrafluoroethylene membrane microfilters with a pore size of 1.0 μm. All nanoscale thin films of the polymer were prepared by spin-coating of the solution on precleaned silicon substrates with and without metal electrode depositions at 2500 rpm for 60 s and subsequent drying in vacuum at 80 °C for 8 h. The thicknesses of the obtained PI films were determined to be in the range 20−40 nm using a spectroscopic ellipsometer (model M2000, Woollam). For devices, aluminum (Al) and Au bottom electrodes with a thickness of 10−300 nm were prepared by E-beam sputtering on precleaned silicon substrates with a thermal oxide layer of 500 nm thickness, while Al top electrodes with a thickness of 10−300 nm were prepared by thermal evaporation through shadow masks under a pressure of 10^{-6} Torr. Each Al top electrode had a size of 0.04 mm^2 (see Figure S1 in the Supporting Information). The current−voltage (I−V) measurements were carried out using a Keithley 4200 semiconductor analyzer with a maximum current compliance of 0.105 A. All the experiments were performed at room temperature under ambient conditions and also carried out with varying temperature in nitrogen atmosphere. In addition, atomic force microscopy (AFM) surface images were obtained using a tapping mode atomic force microscope (Digital Instruments, model Multimode AFM Nanoscope IIIa) equipped with a cantilever which has 26 N/m spring constant and 268 kHz resonance frequency.

Synchrotron X-ray reflectivity (XR) measurements were performed at the 3C1 and 8C1 POSCO beamlines[13] of the Pohang Accelerator Laboratory (PAL).[14] A Si(111) double-crystal monochromator was used to select a wavelength λ of 0.1541 nm with an energy resolution of $\Delta\lambda/\lambda = 5 \times 10^{-4}$, and a Sagittal bender for the second crystal was used to focus the X-ray beam in the horizontal direction. The primary beam was defined by four slits before the sample, and another two slits were used as receiving slits after the sample. The beam was collimated at the sample position to 2 mm (horizontal) by 0.1 mm (vertical). The measured reflected intensity was normalized to the intensity of the primary beam, which was monitored with an ionization chamber. Specular reflection was measured in θ−2θ scanning mode. The reflectivity R, i.e., the ratio of the reflected beam intensity to the primary beam intensity, was measured down to just above 10^{-8}. To obtain accurate determinations of the critical angle of the silicon substrate and of the thin film, 2θ was scanned at small increments of 0.01° at angles smaller than 1.0°. At higher angles, the step width was increased to 0.02−0.1°. The obtained data underwent data binning, geometrical correction, and a background subtraction procedure described in literature.[13,15]

Grazing-incidence X-ray scattering (GIXS) measurement was performed at the PAL 4C2 beamline.[16,17] Measurements were performed at

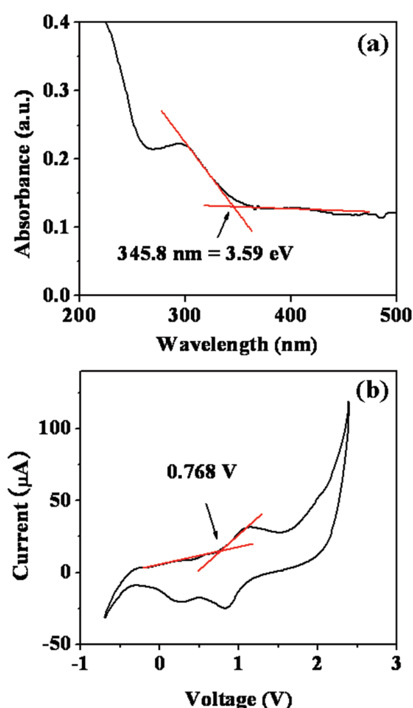

Figure 2. (a) UV−vis spectrum of a 6F-HAB-AM PI film coated on a quartz substrate; (b) CV response of a 6F-HAB-AM PI film fabricated with an Au electrode supported by a silicon substrate in acetonitrile containing 0.1 M tetrabutylammonium tetrafluoroborate. The CV measurements were carried out using an electrochemical workstation (IM6ex impedance analyzer) with a platinum gauze counter electrode and an Ag/AgCl (3.8 M KCl) reference electrode. A scan rate of 100 mV/s was used.

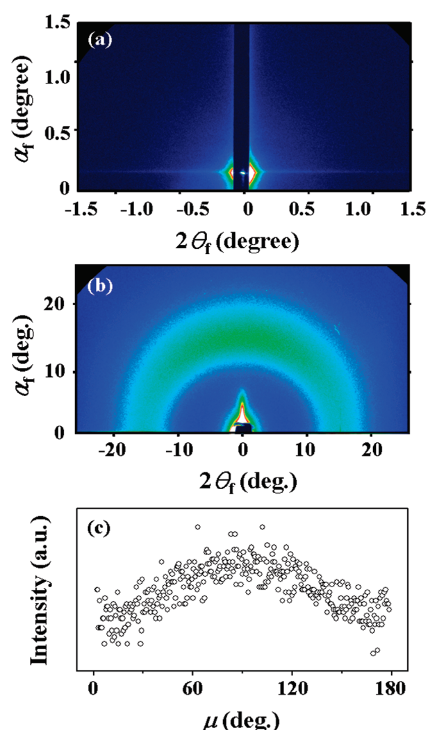

Figure 3. (a) Synchrotron 2D GISAXS pattern measured at 25 °C with α_i = 0.159° for a 40 nm thick 6F-HAB-AM PI film deposited on a silicon substrate; (b) 2D GIWAXS pattern measured with α_i = 0.147°. (c) Azimuthal scattering profile extracted from the 2D GIWAXS pattern in (b) along the amorphous halo ring.

a sample-to-detector distance (SDD) of 125 mm for grazing incidence wide-angle X-ray scattering (GIWAXS) and 2220 mm for grazing incidence small-angle X-ray scattering (GISAXS). Scattering data were typically collected for 30 s using an X-ray radiation source of λ = 0.138 nm with a two-dimensional (2D) charge-coupled detector (CCD; Roper Scientific, Trenton, NJ, USA). The incidence angle α_i of the X-ray beam was set at 0.147° for wide-angle scattering and 0.159° for small-angle scattering, which are between the critical angles of the PI film and the silicon substrate ($\alpha_{c,f}$ and $\alpha_{c,s}$). Scattering angles were corrected according to the positions of the X-ray beams reflected from the silicon substrate with respect to a precalibrated silver behenate powder (TCI, Japan). Aluminum foil pieces were applied as a semitransparent beam stop because the intensity of the specular reflection from the substrate was much stronger than the scattering intensity of the polymer films near the critical angle.

RESULTS AND DISCUSSION

In this study, soluble 6F-HAB PI was synthesized directly from the polycondensation of the respective monomers using isoquinoline as a catalyst. Its ^{1}H NMR spectrum showed the proton peak of the hydroxyl side groups at 10.10 ppm and the characteristic peaks of the aromatic rings in the range of 7.10−8.30 ppm but did not reveal any amino protons originating from possible amic acid residues of partially imidized polymer chains (data given in Experimental Section), confirming that 6F-HAB PI was successfully synthesized. The 6F-HAB PI was determined to have a weight-averaged molecular weight ($\overline{M_w}$) of 36 300 and a polydispersity index (PDI) of 1.9 by GPC analysis. Further, the anthracene was incorporated into the 6F-HAB PI polymer, producing 6F-HAB-AM PI, a new polyimide containing two anthracene groups per chemical repeat unit. The obtained PI product was found to reveal the proton peak of the methyl linkers over the range 6.30 ppm and the characteristic peaks of the aromatic rings in the range 8.61−7.40 ppm but did not reveal any hydroxyl protons (data given in the Experimental Section), confirming that the anthracene containing PI was successfully synthesized. The new functional PI was soluble in some common solvents, providing good quality thin films by means of a conventional solution spin-casting and subsequent drying process. Thin films of this PI were determined to have smooth surfaces (0.27 nm root-mean square (rms) roughness) by means of AFM analysis (Figure S2 in the Supporting Information).

The TGA analysis found that 5% weight loss temperature of 6F-HAB-AM PI was measured at 410 °C (data not shown). The DSC measurements could not find glass transition up to 250 °C (Figure S3 in the Supporting Information), suggesting that the PI may have a glass transition temperature T_g of >250 °C. These results confirm that the 6F-HAB-AM PI is a dimensionally, thermally stable polymer, as commonly observed for the conventional PIs used in industry.[12,18]

6F-HAB-AM PI films were investigated by UV−vis spectroscopy and CV analysis. Figure 2 shows UV−vis spectroscopy and CV data for the PI films. From the UV−vis spectrum in Figure 2a, the band gap (i.e., the difference between the highest occupied molecular orbital (HOMO) level and the lowest unoccupied molecular orbital (LUMO) level) for the polymer is estimated to be 3.59 eV. From the CV data (Figure 2b), the oxidation onset potential (E_{ox}) for the 6F-HAB-AM PI is

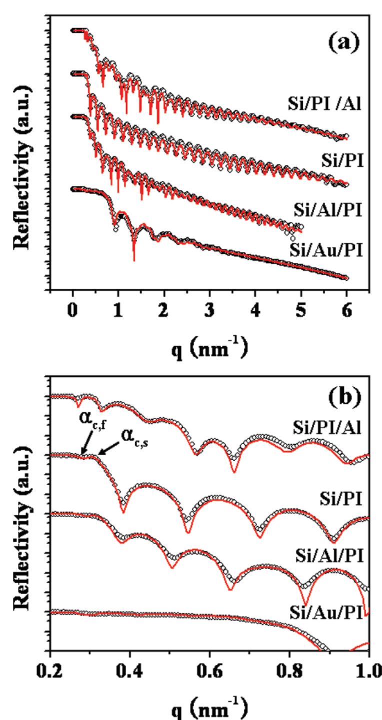

Figure 4. Synchrotron X-ray reflectivity (XR) profiles of 6F-HAB-AM PI thin films in contact with silicon substrate, Al bottom electrode, Au bottom electrode, and Al top electrode: (a) whole measured data (symbols) with fitting curves (solid lines); (b) the measured and fitted data in the low angle region were enlarged. $\alpha_{c,f}$ and $\alpha_{c,s}$ denote the critical angles of the PI film and Si substrate, respectively.

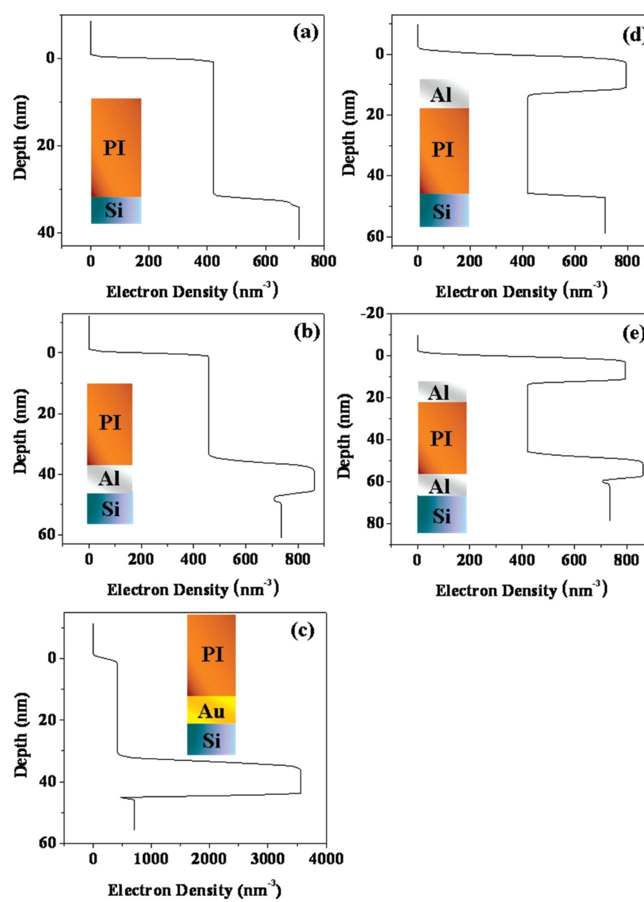

Figure 5. Electron density profiles of the PI-based thin films 6F-HAB-AM PI thin films in contact with silicon substrate, Al bottom electrode, Au bottom electrode, and Al top electrode, which were obtained by analysis of the XR data in Figure 4: (a) PI coated onto Si substrate; (b) PI coated onto the Al bottom electrode supported with Si substrate; (c) PI coated onto the Au bottom electrode supported with Si substrate; (d) Al top electrode thermally deposited onto the PI film supported with Si substrate; (e) Al/PI/Al, which was made by the combination of the electron density profiles in (b) and (d).

determined to be 0.77 V vs Ag/AgCl electrode. The external ferrocene/ferrocenium (F_c/F_{c+}) redox standard potential ($E_{1/2}$) was measured to be 0.48 V vs Ag/AgCl electrode in acetonitrile. Assuming that the HOMO level for the F_c/F_{c+} standard is −4.80 eV with respect to the zero vacuum level, the HOMO level for the 6F-HAB-AM PI is determined to be −5.09 eV. Therefore, the LUMO level of the 6F-HAB-AM PI is estimated to be −1.50 eV.

The structure of 6F-HAB-AM PI in nanoscale thin films was examined by synchrotron GIXS analysis. Figure 3a shows a representative 2D GISAXS pattern measured for the polymer thin films supported with silicon substrates. As can be seen in the figure, the polymer reveals a featureless scattering pattern, indicating that no discernible nanostructure or microstructure was developed in the nanoscale thin film. Figure 3b displays a representative 2D GIWAXS patter of the polymer films. This scattering pattern shows only a broad, weak scattering ring like amorphous halo. The scattering ring is determined to have a *d*-spacing of 0.502 nm, which corresponds to the mean interchain distance of 6F-HAB-AM PI molecules. Further, here, it is noted that the scattering ring is apparently anisotropic. Thus, an azimuthal scattering profile has been extracted from the 2D scattering pattern along the amorphous halo ring, and the resulting profile is displayed in Figure 3c as a function of azimuthal angle μ. As can be seen in the figure, the scattering intensity shows the maximum value at μ = 90° and decreases toward μ = 0° and 180°. The scattering results indicate that the 6F-HAB-AM PI molecules orient preferentially in the plane of the nanoscale thin films rather than randomly.

In device fabrications, 6F-HAB-AM PI is physically contacted with metal electrodes. Thus, one may be concerned about delamination at the interfaces in the device. However, no delamination was observed at the interfaces of the polymer film in contact with the bottom and top metal electrodes through the entire device fabrication process and electrical performance tests. Furthermore, one may be concerned about diffusion of the atoms and/or ions of metal electrodes into the polymer layer and further about oxide layer formation at the metal electrode surfaces through the post polymer coating process and its influence onto the device performance. To check these, the PI films were prepared in contact with silicon substrate and top and bottom metal electrodes, and then, their interface was investigated using synchrotron X-ray reflectivity analysis. The measured XR profiles are shown in Figure 4a; the XR profiles in the low-angle region are magnified in Figure 4b. As shown in the figures, the XR profiles can be satisfactorily fitted with the Parratt's fitting algorithm.[13,19] From these XR analyses, the electron density profile across the film thickness and other structural parameters were obtained. The results are summarized in Figure 5 and Table 1.

For the PI film deposited onto the Al bottom electrode, the XR analysis found that an aluminum oxide layer forms with a

Table 1. Structural Parameters and Electron Density Profiles of Various Bilayer Samples Prepared from the PI film, Silicon Substrate, Al Electrode, and Au Electrode

	substrate or bottom layer			PI layer			top layer			interlayer[d]		
sample (bottom/top)	d^a (nm)	ρ_e^b (nm^{-3})	σ^c (nm)	d^a (nm)	ρ_e^b (nm^{-3})	σ^c (nm)	d^a (nm)	ρ_e^b (nm^{-3})	σ^c (nm)	d^a (nm)	ρ_e^b (nm^{-3})	σ^c (nm)
Si/PI		692.5	0.4	32.2	420.2	0.2				1.72	676.2	0.4
Al/PI	10.4	795.6	1.0	36.1	420.2	0.4				1.2	473.0	0.4
Au/PI	11.2	3560.6	0.9	33.3	420.2	0.6						
PI/Al				34.2	420.2	1.5	11.2	795.6	0.9	0.7	528.7	0.6

[a] Layer thickness. [b] Electron density of layer. [c] Roughness of layer in contact with air or upper layer. [d] Silicon oxide layer for Si(bottom)/PI(top), aluminum oxide layer for Al/PI, and PI−Al mixed layer (which is due to the roughness of interface) for PI/Al systems.

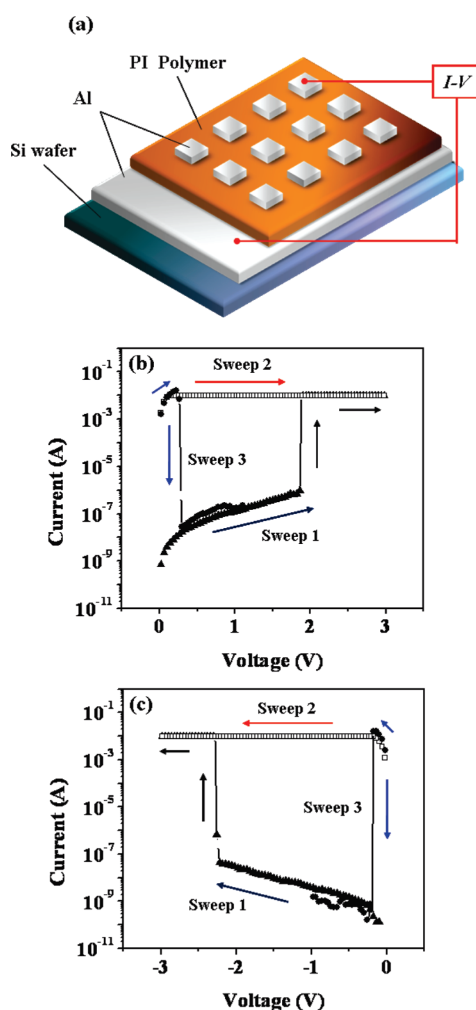

Figure 6. (a) Schematic diagram of the memory device fabricated with the PI and aluminum top and bottom electrodes. Representative $I-V$ curves for Al/6F-HAB-AM PI(20 nm thick)/Al devices in unipolar switching mode: (b) the first sweep was performed with a current compliance of 0.01 A from 0 to +3.0 V to switch the device on, the second sweep was performed with the same current compliance (0.01 A) from 0 to +3.0 V to test the ON-state of the device, and the third sweep was carried out with a current compliance of 0.1 A to switch the device off; (c) the first sweep was performed with a current compliance of 0.01 A from 0 to −3.0 V to switch the device on, the second sweep was performed with the same current compliance (0.01 A) from 0 to −3.0 V to test the ON-state of the device, and the third sweep was carried out with a current compliance of 0.1 A to switch the device off. The electrode contact area was 0.2 × 0.2 mm^2.

thickness of 1.2 nm and an rms surface roughness of 0.4 nm during the polymer deposition process while the deposited polymer film has a thickness of 36.1 nm and an rms surface roughness of 0.4 nm (Figure 5a,b, and Table 1). In comparison, the PI film, which was deposited onto the Au bottom layer, was found to have 33.3 nm thickness and 0.6 nm rms surface roughness (Figure 5c and Table 1). These PI film characteristics are similar to those of the film deposited onto the Al bottom electrode although the surface roughness is relatively high because of the relatively rough surface of the Au bottom electrode.

In addition, the interface of Al top electrodes deposited onto the PI films was investigated by XR analysis (Figure 5d and Table 1). The PI film (bottom layer) was determined to have an rms roughness of 1.5 nm. Surprisingly, this film roughness is much higher than that (0.2 nm) before the Al top layer deposition. This result indicates that the Al deposition onto the PI via thermal evaporation process causes the polymer film somewhat rough. Such high surface roughness might be originated from bombardments of Al atoms and their aggregates with high thermal energies to the polymer film surface during the thermal evaporation process. On the other hand, the thickness of the interface between the PI film and the Al top electrode was found to be only 0.7 nm. This interfacial thickness is very thin. Even though there is such a very thin thickness, its electron density (528.7 electrons per nm^3) is larger than that (473 electrons per nm^3) of the oxide layer formed at the Al bottom electrode. Further, the Al top electrode was deposited onto the PI film in vacuum. These results collectively suggest that no aluminum oxide layer was formed between the PI film and the Al top electrode and the very thin interfacial layer observed between the layers is attributed to the mechanical mixing of the two layers occurring in the rough surface of the PI film. Finally, we combined the XR analysis data of the Al/PI and PI/Al samples together, producing a whole electron density profile of the Al/PI/Al devices as demonstrated in Figure 5e.

With the above structure, interface, and property details, devices were fabricated with the thin PI films and electrodes of Al and Au (Figure 6a) and their memory performance was tested. Figure 6b shows the typical $I-V$ characteristics of bistable memory devices fabricated with 20 nm thick 6F-HAB-AM PI films as active layer and Al as top and bottom electrodes. As can be seen in the figure, the as-fabricated 6F-HAB-AM PI film initially exhibits a high-resistance state (OFF-state). However, when a positive voltage is applied with a current compliance of 0.01 A, an abrupt increase of current occurs in the device near +1.86 V (which corresponds to the critical voltage to switch the device on), indicating that the device undergoes a sharp electrical

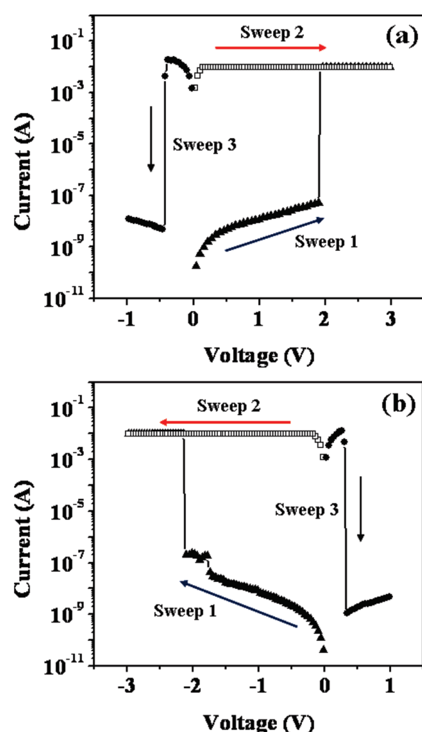

Figure 7. Representative $I-V$ curves of Al/6F-HAB-AM PI(20 nm thick)/Al devices in bipolar mode: (a) the first sweep was performed with a current compliance of 0.01 A from 0 to +3.0 V to switch the device on, the second sweep was performed with the same current compliance (0.01 A) from 0 to +3.0 V to test the ON-state of the device, and the third sweep from 0 to −1.0 V was carried out with a current compliance of 0.1 A to switch the device off; (b) the first sweep was performed with a current compliance of 0.01 A from 0 to −3.0 V to switch the device on, the second sweep was performed with the same current compliance (0.01 A) from 0 to −3.0 V to test the ON-state of the device, and the third sweep from 0 to +1.0 V was carried out with a current compliance of 0.1 A to switch the device off.

transition from the OFF-state to a high conductivity state (ON-state). This OFF-to-ON transition can function in a memory device as a "writing" process. Once the device has reached its ON-state, it remains there, even after the power is turned off or during sequential reverse and forward voltage sweeping with the current compliance maintained at 0.01 A.

The device in the ON-state can be switched off (i.e., returned to the OFF-state) by applying a positive voltage with a current compliance of 0.1 A, which is 10 times higher than the current compliance for the switch-ON process (namely, the writing process). As shown in Figure 6b, when a positive voltage is again applied with a current compliance of 0.1 A, there is an abrupt decrease in the current in the device around +0.28 V (which corresponds to the critical voltage to switch the device off), which indicates that the device undergoes a sharp electrical transition from the ON-state to the OFF-state. The ON/OFF current ratio of the device is in the range 10^4 to 10^7, depending on the turn-ON compliance current and the reading voltage; a higher turn-ON compliance current and a lower reading voltage result in a higher ON/OFF current ratio.

Similar ON and OFF switching behaviors were observed for the device when sweeping with a negative voltage (Figure 6c), although the switching ON occurred at a slightly higher voltage of −2.20 V and the ON/OFF current ratio of the range of 10^5 to 10^7. These results indicate that the 6F-HAB-AM PI film in the device exhibits excellent unipolar ON and OFF switching behavior regardless of the sweep direction (i.e., independent of polarity).

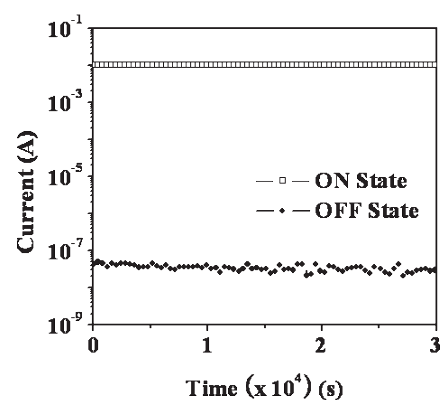

Figure 8. Long-time responses (i.e., retention times) of the ON- and OFF-states of the Al/6F-HAB-AM PI/Al device, probed under a constant bias of +0.5 V. The ON-state ("write") was induced with a turn-on compliance current of 0.005 A by applying a voltage of +2.5 V, and the OFF-state ("erase") was reinstated with a turn-off compliance current of 0.1 A by applying a voltage of 1.0 V.

Taking these electrical switching behaviors into account, the ON and OFF switching behavior of the 6F-HAB-AM PI-based devices were further tested by applying voltage biases sequentially through both positive and negative polarities; i.e., either a positive or a negative voltage is applied first with a current compliance of 0.01 A to switch the device on, and then, the opposite voltage is applied with a current compliance of 0.1 A to switch the device off. Figure 7a shows the typical ON and OFF switching characteristics of the Al/PI/Al device. As can be seen in the figure, the as-fabricated 6F-HAB-AM PI film initially exhibits the OFF-state. However, when a positive voltage is applied with a current compliance of 0.01 A, the device undergoes a sharp electrical transition from the OFF-state to the ON-state with a current of approximately +1.92 V. Once the device has reached its ON-state, it remains there, even after the power is turned off and during back and forth voltage sweeping at the same polarity with the current compliance maintained at 0.01 A. Moreover, the ON-state of the device was found to persist even during back and forth voltage sweeping with a negative polarity with the current compliance maintained at 0.01 A (data not shown). The device in the ON-state was found to be switched off by applying the opposite voltage with a current compliance of 0.1 A. As shown in Figure 7a, when a negative voltage is applied with a current compliance of 0.1 A, the device exhibits a sharp electrical transition from the ON-state to the OFF-state with a current of approximately −0.42 V. Similar ON and OFF switching behaviors were observed for the devices when the initial switch-ON sweeping was carried out with a negative voltage (Figure 7b). These results indicate that the 6F-HAB-AM PI film in the device further exhibits excellent bipolar ON and OFF switching behavior (i.e., dependent on polarity).

Figure 8 shows representative results of the stability tests for the ON- and OFF-state (namely, retention tests), which were carried out on the device at room temperature in ambient conditions using a reading voltage of +0.5 V. As can be seen in the figure, once the device is switched to the ON-state by applying a voltage of +2.5 V with a compliance current of 0.01 A, the

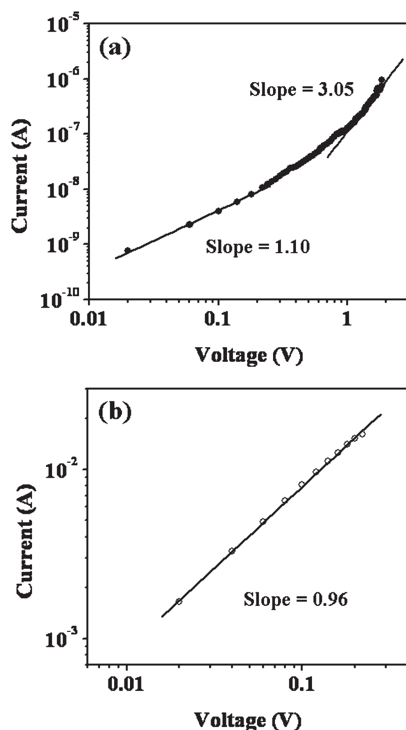

Figure 9. Experimental (circles) and fitted (solid lines) $I-V$ curves for the Al/6F-HAB-AM PI/Al device: (a) OFF-state with the Ohmic (below 1.0 V) and the trap-limited SCLC (around 1.0 V) conduction model. (b) ON-state with the Ohmic current model.

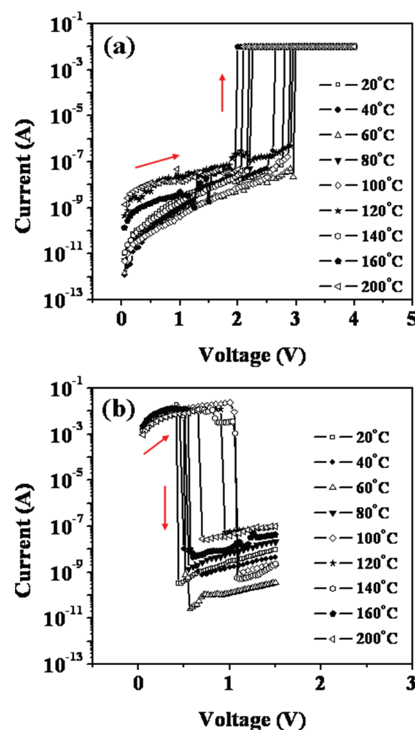

Figure 10. Representative $I-V$ curves for Al/6F-HAB-AM PI(20 nm thick)/Al devices at various temperatures up to 200 °C: (a) the turn-ON process was performed with a current compliance of 0.01 A from 0 to +4.0 V; (b) the turn-OFF process was carried out with a current compliance of 0.1 A from 0 to +1.5 V. The electrode contact area was 0.2 × 0.2 mm^2.

ON-state is retained without any degradation for a test period of 3.0×10^4 s. Moreover, it was confirmed that the device stays in the ON-state for 4 months to a year. When the ON-state is switched back to the OFF-state by applying a voltage of +0.8 V with a compliance current of 0.1 A, the OFF-state also persists without any degradation for the whole test period and further. Overall, the device exhibits excellent reliability, even in ambient conditions.

To investigate the electrical switching characteristics of our devices, the measured $I-V$ data was further analyzed in detail using various conduction models.[20−22] The trap-limited space-charge-limited conduction (SCLC) model[20] was found to fit the $I-V$ data for the OFF-state very well (Figure 9a). These results indicate that the trap-limited SCLC mechanism is dominant in the OFF-state of the device. The Ohmic contact model[21] was found to satisfactorily fit the $I-V$ data for the ON-state (Figure 9b), indicating that Ohmic conduction is dominant in the ON-state of the device.

The above results suggest that the excellent unipolar and bipolar ON and OFF switching behaviors of the 6F-HAB-AM PI films are governed by trap-limited SCLC and local filament formation. The trapping sites might arise due to the chemical composition of the 6F-HAB-AM PI chain, which has two anthracene moieties, a trifluoromethyl group, and two imide rings per repeat unit of the backbone. In general, polyimides are the materials with extremely low conductivity.[23] However, the anthracene side groups of the 6F-HAB-AM PI are hole-transporting (i.e., electron donating) moieties. Thus, to determine the contributions of the anthracene moieties of the 6F-HAB-AM PI to the observed electrical switching behaviors, we fabricated and tested devices with 6F-HAB PI, which has the same backbone as 6F-HAB-AM PI but does not contain anthracene moieties. None of the 6F-HAB PI-based devices was found to exhibit electrically bistable characteristics.[24] These results suggest that the anthracene moieties play a key role in the observed electrical switching properties of the 6F-HAB-AM PI-based devices. In particular, the anthracene moieties are likely to act as hole trapping sites, so the anthracene moieties in the 6F-HAB-AM PI film will become enriched with holes when a bias with a set current compliance (for example, 0.01 A) is applied to the PI film. At the same time, the trifluoromethyl groups and imide rings in the PI film will act as electron trapping sites and become enriched with electrons. When the applied bias reaches the threshold voltage, the trapped charges are able to move through the trapped sites by means of a hopping process (i.e., through filament formation), which results in current flow between the bottom and top electrodes under the chosen current compliance. When a bias is again applied to the device in the ON-state with another current compliance set at a current level (for example, 0.1 A) that is higher than the turn-on compliance current (0.01 A), a large number of charges can flow through the previously formed filaments and this large current flow is likely to produce heat. As discussed above for the 6F-HAB-AM PI, the energy barrier to hole injection is lower than that to electron injection, so conduction in the 6F-HAB-AM PI device is dominated by hole injection. Furthermore, the number of charge carriers injected into the PI film increases with increases in the applied voltage bias. At biases greater than a certain voltage, the number of injected charges is too high, which overloads the capacity of the filaments. The excess injected charges are probably trapped in the PI layer as well as in the PI/electrode interface. Further, such excess current is likely to

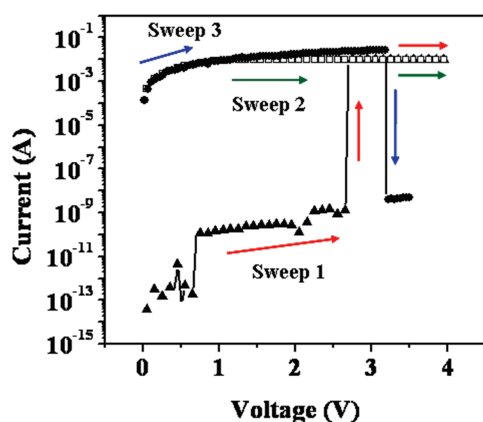

Figure 11. Representative $I-V$ curves for Au/6F-HAB-AM PI(20 nm thick)/Al devices in unipolar switching mode: the first sweep was performed with a current compliance of 0.01 A from 0 to +4.0 V to switch the device on, the second sweep was performed with the same current compliance (0.01 A) from 0 to +4.0 V to test the ON-state of the device, and the third sweep was carried out with a current compliance of 0.1 A to switch the device off.

produce additional heat and, at the same time, result in repulsive Coulomb interactions with the charges trapped locally within the PI layer and in the interface. The generated heat and repulsive Coulomb interactions then cause rupture of the filaments formed in the switch-ON process. As a result, the device returns to its initial OFF-state.

The device was further investigated to confirm its thermal stability. Figure 10 shows the representative $I-V$ characteristics of an Al/PI/Al device at various temperatures. As can be seen in the figure, the ON-state current level of the device does not change when the device temperature is raised up to 200 °C. Further, the switching characteristics (i.e., nonvolatile memory behavior) of the device are retained up to 200 °C. Moreover, the turn-ON voltage of the device varies little with temperature, showing no apparent correlation with the temperature variation. These results indicate that the 6F-HAB-AM PI devices have high temperature stability and retain excellent nonvolatile memory performance up to 200 °C. On the other hand, the OFF-state current level of the device was found to generally increase with increasing temperature. The OFF-state current varies little with increasing temperature until around 100 °C and then increases rapidly with further increases in temperature. However, the $I-V$ characteristic of the OFF-state was found to be still governed by the trap-limited SCLC. Thus, the increases in the OFF-state current might result from the increase of hopping rate due to high thermal excitations.[25] The turn-OFF voltage of the device also varies little with temperature, showing no apparent correlation with the temperature variation. The overall results indicate that the PI is highly reliable as a storage device component even at high temperatures.

As discussed above, the XR analysis found that the PI film formation process causes oxidation of the Al bottom electrode, resulting in a very thin oxide layer (1.2 nm) formation at the electrode surface. However, aluminum or ion diffusion into the polymer layer was not detected. Thus, the PI device system was further studied to ascertain whether the observed resistive switching behavior of the 6F-HAB-AM PI device is due to the 6F-HAB-AM PI or the oxide layer (Al_2O_3) that might form during the fabrication of the polymer film. For this, we fabricated devices with the PI films by substituting the Al bottom electrode with gold (Au), because as a noble metal the Au is quite inert and cannot easily be oxidized,[23] and tested them. As shown in Figure 11, the device with Au bottom electrode (Au/PI/Al device) was found to exhibit resistive switching behavior similar to that of the device with Al bottom electrode. The ON/OFF current ratio of the device is in the range of 10^6 to 10^9, depending on the turn-ON compliance current and the reading voltage; a higher turn-ON compliance current and a lower reading voltage result in a higher ON/OFF current ratio. These results indicate that the oxide layer might not affect significantly the resistive switching characteristics of the Al/PI/Al device.

Further, the Au/PI/Al device showed noticeable features as follows. The turn-OFF has occurred at a voltage higher than the turn-ON voltage (Figure 11). Meanwhile, the turn-OFF process occurred at the current level similar to the turn-OFF current of the Al/PI/Al device. Also, the ON-state resistance of the Au/PI/Al device is higher than that of the Al/PI/Al device, so that the current level of the Au/PI/Al device has reached the turn-OFF level at higher voltage. These features collectively indicate that the turn-OFF process of the device with 6F-HAB-AM PI is closely related to current level rather than voltage level. Moreover, these phenomena also support that the conduction mechanism of the PI-based devices is related to the formation and rupture of filaments.

CONCLUSIONS

In this study, we prepared an aromatic polyimide, 6F-HAB-AM PI. This polymer is amorphous and orients preferentially in the plane of nanoscale thin films, and the polymer exhibits high thermal and dimensional stability, which are required for fabrications of devices with high reliability. Devices were fabricated using the polyimide as an active layer and Al bottom and top electrodes. The memory devices were found to operate in electrically bistable unipolar and bipolar switching modes over a very small voltage range, less than ±2 V by controlling the compliance current. The devices were found to be repeatedly written, read, and erased with long reliability in air ambient conditions as well as at temperatures up to 200 °C. The devices exhibit a high ON/OFF current ratio of 10^4-10^7, depending on the turn-ON compliance current and the reading voltage; a higher turn-on compliance current and a lower reading voltage result in a higher ON/OFF current ratio. The experimental results (the $I-V$, UV−vis, and CV results for the active PI layer and the work functions of the electrodes) of this study suggest that these nonvolatile memory devices operate electrically according to a mechanism involving trap-limited SCLC conduction and local filament formation. Synchrotron XR analysis found that an aluminum oxide layer is formed with a thickness of 1.2 nm at the Al bottom electrode during the post PI film deposition process because of the high oxidation ability of aluminum. However, such a thin oxide layer could make no significant influence to the nonvolatile memory device performance. Overall, this study has demonstrated that the thermally, dimensionally stable 6F-HAB-AM PI is a very suitable active material for the mass production at low cost of high performance, programmable nonvolatile memory devices that can be operated with very low power consumption in excellent unipolar and bipolar ON and OFF switching modes with a high ON/OFF switching ratio and high thermal and dimensional stability.

ASSOCIATED CONTENT

S Supporting Information. Optical microscope images of a device, atomic force microscopy image of a 6F-HAB-AM PI film, and differential scanning calorimetry data (three figures). This material is available free of charge via the Internet at http://pubs.acs.org.

AUTHOR INFORMATION

Corresponding Author

*Tel: +82-54-279-2120. Fax: +82-54-279-3399. E-mail: ree@postech.edu.

Author Contributions

†S.P. and K.K. contributed equally to this work.

ACKNOWLEDGMENT

This study was supported by the National Research Foundation (NRF) of Korea of the Ministry of Education, Science and Technology (MEST) (am and Center for Electro-Photo Behaviors in Advanced Molecular Systems) and the MEST (BK21 Program and World Class University Program). Synchrotron GIXS and XR measurements were supported by MEST, POSCO, and POSTECH Foundation.

REFERENCES

(1) (a) Donhauser, Z. J.; Mantooth, B. A.; Kelly, K. F.; Bumm, L. A.; Monnell, J. D.; Stapleton, J. J.; Price, D. W., Jr.; Rawlett, A. M.; Allara, D. L.; Tour, J. M.; Weiss, P. S. *Science* **2001**, *292*, 2303. (b) Gao, H. J.; Sohlberg, K.; Xue, Z. Q.; Chen, H. Y.; Hou, S. M.; Ma, L. P.; Fang, X. W.; Pang, S. J.; Pennycook, S. J. *Phys. Rev. Lett.* **2000**, *84*, 1780. (c) Aviram, A.; Joachim, C.; Pomerantz, M. *Chem. Phys. Lett.* **1988**, *146*, 490. (d) Chen, J.; Ma, D. *Appl. Phys. Lett.* **2005**, *87*, 23505. (e) Tu, C.-H.; Lai, Y.-S.; Kwong, D.-L. *Appl. Phys. Lett.* **2006**, *89*, 062105.

(2) (a) Elsharkawi, A. R.; Kao, C. *J. Phys. Chem. Solids* **1977**, *38*, 95. (b) Chiang, C. *Solid State Commun.* **1981**, *39*, 111.

(3) Kolosov, D.; English, D. S.; Bulovic, V.; Barbara, P. F.; Forrest, S. R.; Thompson, M. E. *J. Appl. Phys.* **2001**, *90*, 3242.

(4) Liu, Z.; Yasseri, A. A.; Lindsey, J. S.; Bocian, D. F. *Science* **2003**, *302*, 1543.

(5) Ma, D.; Aguiar, M.; Freire, J. A.; Hümmelgen, I. A. *Adv. Mater.* **2000**, *12*, 1063.

(6) (a) Baek, S.; Lee, D.; Kim, J.; Hong, S.-H.; Kim, O.; Ree, M. *Adv. Funct. Mater.* **2007**, *17*, 2637. (b) Lee, D.; Baek, S.; Ree, M.; Kim, O. *Jpn. J. Appl. Phys.* **2008**, *47*, 5665. (c) Lee, D.; Baek, S.; Ree, M.; Kim, O. *Electron. Lett.* **2008**, *44*, 596. (d) Lai, Y.-S.; Tu, C.-H.; Kwong, D.-L.; Chen, J. S. *Appl. Phys. Lett.* **2005**, *87*, 122101. (e) Lai, Y.-S.; Tu, C.-H.; Kwong, D.-L.; Chen, J. S. *IEEE Electron Device Lett.* **2006**, *27*, 451.

(7) Lee, T. J.; Park, S.; Hahm, S. G.; Kim, D. M.; Kim, K.; Kim, J.; Kwon, W.; Kim, Y.; Chang, T.; Ree, M. *J. Phys. Chem. C* **2009**, *113*, 3855.

(8) (a) Majumdar, H. S.; Bandyopadhyay, A.; Bolognesi, A.; Pal, A. J. *J. Appl. Phys.* **2002**, *91*, 2433. (b) Teo, E. Y. H.; Ling, Q. D.; Song, Y.; Tan, Y. P.; Wang, W.; Kang, E. T.; Chan, D. S. H.; Zhu, C. *Org. Electron.* **2006**, *7*, 173.

(9) Lim, S. L.; Ling, Q.; Teo, E. Y. H.; Zhu, C. X.; Chan, D. S. H.; Kang, E.-T.; Neoh, K. G. *Chem. Mater.* **2007**, *19*, 5148.

(10) (a) Ling, Q.; Song, Y.; Ding, S. J.; Zhu, C.; Chan, D. S. H.; Kwong, D.-L.; Kang, E.-T.; Neoh, K. G. *Adv. Mater.* **2005**, *17*, 455. (b) Xie, L.-H.; Ling, Q.-D.; Hou, X.-Y.; Huang, W. *J. Am. Chem. Soc.* **2008**, *130*, 2120. (c) Karakawa, M.; Chikamatsu, M.; Yoshida, Y.; Azumi, R.; Yase, K.; Nakamoto, C. *Macromol. Rapid Commun.* **2007**, *28*, 1479. (d) Majee, S. K.; Majumdara, H. S.; Bolognesi, A.; Pal, A. J. *Synth. Met.* **2006**, *156*, 828. (e) Kim, T.-W.; Lee, K.; Oh, S.-H.; Wang, G.; Kim, D.-Y.; Jung, G.-Y.; Lee, T. *Nanotechnology* **2008**, *19*, 405201.

(11) Hahm, S. G.; Choi, S.; Hong, S.-H.; Lee, T. J.; Park, S.; Kim, D. M.; Kwon, W.-S.; Kim, K.; Kim, O.; Ree, M. *Adv. Funct. Mater.* **2008**, *18*, 3276.

(12) (a) Zhu, J.; Wei, S.; Alexander, M. J.; Dang, T. D.; Ho, T. C.; Guo, Z. *Adv. Funct. Mater.* **2010**, *18*, 3076. (b) Zhu, J.; Wei, S.; Chen, X.; Karki, A. B.; Rutman, D.; Young, D. P.; Guo, Z. *J. Phys. Chem. C* **2010**, *114*, 8844.

(13) (a) Bolze, J.; Ree, M.; Youn, H. S.; Chu, S.-H.; Char, K. *Langmuir* **2001**, *17*, 6683. (b) Hwang, Y.; Heo, K.; Chang, C. H.; Joo, M. K.; Ree, M. *Thin Solid Films* **2006**, *510*, 159.

(14) (a) Ree, M.; Nam, S. H.; Yoon, M.; Kim, B.; Kim, K.-R.; Kang, T.-H.; Kim, J.-Y.; Kim, K.-J.; Shin, T. J.; Lee, H.-S.; Park, S.-J.; Kim, N.; Lee, K.-B.; Ko, I.-S.; Namkung, W. *Synchrotron Radiat. News* **2009**, *22*, 4. (b) Ree, M.; Ko, I.-S. *Phys. High Tech.* **2005**, *14*, 2.

(15) Salah, F.; Harzallah, B.; van der Lee, A. *J. Appl. Crystallogr.* **2007**, *40*, 813.

(16) (a) Yoon, J.; Kim, K.-W.; Kim, J.; Heo, K.; Jin, K. S.; Jin, S.; Shin, T. J.; Lee, B.; Rho, Y.; Ahn, B.; Ree, M. *Macromol. Res.* **2008**, *16*, 575. (b) Lee, B.; Park, Y.-H.; Hwang, Y.; Oh, W.; Yoon, J.; Ree, M. *Nat. Mater.* **2005**, *4*, 147. (c) Lee, B.; Oh, W.; Hwang, Y.; Park, Y.-H.; Yoon, J.; Jin, K. S.; Heo, K.; Kim, J.; Kim, K.-W.; Ree, M. *Adv. Mater.* **2005**, *17*, 696.

(17) (a) Yoon, J.; Jin, K. S.; Kim, H. C.; Kim, G.; Heo, K.; Jin, S.; Kim, J.; Kim, K.-W.; Ree, M. *J. Appl. Crystallogr.* **2007**, *40*, 476. (b) Yoon, J.; Lee, S. W.; Choi, S.; Heo, K.; Jin, K. S.; Jin, S.; Kim, G.; Kim, J.; Kim, K.-W.; Kim, H.; Ree, M *J. Phys. Chem. B* **2008**, *112*, 5338. (c) Kim, G.; Park, S.; Jung, J.; Heo, K.; Yoon, J.; Kim, H.; Kim, I. J.; Kim, J. R.; Lee, J. I.; Ree, M. *Adv. Funct. Mater.* **2009**, *19*, 1631.

(18) (a) Hahm, S. G.; Lee, T. J.; Ree, M. *Adv. Funct. Mater.* **2007**, *17*, 1359. (b) Hahm, S. G.; Lee, T. J.; Chang, T.; Jung, J. C.; Zin, W. C.; Ree, M. *Macromolecules* **2006**, *39*, 5385. (c) Shin, T. J.; Ree, M. *J. Phys. Chem. B* **2007**, *111*, 13894. (d) Hahm, S.; Lee, S. W.; Suh, J.; Chae, B.; Kim, S. B.; Lee, S. J.; Lee, K. H.; Jung, J. C.; Ree, M. *High Perform. Polym.* **2006**, *18*, 549. (e) Ree, M. *Macromol. Res.* **2006**, *14*, 1. (f) Ree, M.; Shin, T. J.; Lee, S. W. *Korea Polym. J.* **2001**, *9*, 1. (g) Ree, M.; Shin, T. J.; Park, Y. H.; Lee, H.; Chang, T. *Korea Polym. J.* **1999**, *7*, 370.

(19) Parratt, L. G. *Phys. Rev.* **1954**, *95*, 359.

(20) Mark, P.; Helfrich, W. *J. Appl. Phys.* **1962**, *33*, 205.

(21) Campell, A. J.; Bradley, D. D. C.; Lidzey, D. G. *J. Appl. Phys.* **1997**, *82*, 6326.

(22) (a) Jessen, K. L. *J. Vac. Sci. Technol., B* **2003**, *21*, 1528. (b) Frenkel, J. *Phys. Rev.* **1938**, *54*, 647. (c) Laurent, C.; Kay, E.; Souag, N. *J. Appl. Phys.* **1988**, *64*, 336.

(23) Viehbeck, A.; Goldberg, M. J.; Kovac, C. A. *J. Electrochem. Soc.* **1990**, *137*, 1460.

(24) Kim, K.; Park, S.; Hahm, S. G.; Lee, T. J.; Kim, D. M.; Kim, J. C.; Kwon, W.; Ko, Y.-G.; Ree, M. *J. Phys. Chem. B* **2009**, *113*, 9143.

(25) Kim, D. M.; Park, S.; Lee, T. J.; Hahm, S. G.; Kim, K.; Kim, J. C.; Kwon, W.; Ree, M. *Langmuir* **2009**, *25*, 11713.